Arch. Metall. Mater. **63** (2018), 2, 765-772

DOI: 10.24425/122402

K. ARKUSZ*#, E. KRASICKA-CYDZIK*

THE EFFECT OF PHOSPHATES AND FLUORIDES, INCLUDED IN TiO_2 NANOTUBE LAYERS ON THE PERFORMANCE OF HYDROGEN PEROXIDE DETECTION

Titania nanotube (TNT) arrays fabricated by anodizing of titanium foil in organic (ethylene glycol) and inorganic (phosphoric acid) electrolytes and thermally modified in argon revealed much improved properties to detect hydrogen peroxide. Horseradish peroxidase and acetate thionine co-absorbed by a dip coating on the TNT electrode were used to detect hydrogen peroxide in phosphate buffered saline. The morphology and electrochemical properties of TNT arrays were studied by scanning electron microscopy, electrochemical impedance spectroscopy and cyclic voltammetry. Well defined oxidation and reduction peaks for potassium ferricyanide have been observed for TNT formed in ethylene glycol and annealed in argon. TNT arrays formed in organic electrolyte and annealed in argon indicated more favorable adsorption and electrochemical properties what was confirmed by detection of hydrogen peroxide towards analyte in phosphorate buffered saline solution.

Keywords: titania nanotubes, thermal modification, biosensor, hydrogen peroxide

1. Introduction

Many analytical methods have been used for detection of hydrogen peroxide, such as electrochemical technique, spectrometry, chromatography and chemiluminescence [1]. Among these methods, amperometric enzyme-based biosensors have received significant attention due to its expediency, high selectivity and sensitivity. Also various materials as biosensor platform and different mediators of electrochemical sensing are used.

In recent years, a significant increase of interest in using nanostructured metal oxides as an immobilization matrix for enzymes, microorganisms, cell carriers [2-3] has been observed. Titania nanotubes (TNT) are a modern and an excellent example of these structures. TNT are considered a very important material due to its promising applications in many fields ranging from energy harvesting to sensors and implantology [4-5]. TNT not only has a high surface area, good biocompatibility, nontoxicity but also does not cause any changes in enzyme structure, stability and specifity of enzyme [6].

TNT can be formed using varying process i.e. electrochemical anodizing [7], through-mask anodization [8], hydrothermal treatment [9]. The electrochemical anodization is the most popular TNT formation technique due to homogenous structure of the obtained TNT and the possibility of its morphological parameter control. Studies to date indicate that the diameter of TNT is directly proportional to the anodizing potential [8] and fluoride concentration [10], the length of TNT depends on anodizing time [8] and pH of electrolyte [11]. Not only anodizing parameters influence the electrochemical properties of TNT but also the electrolyte. The nature of electrolyte affects the migration of fluoride ions on the surface of the electrode and thus, resulting structures are different [8]. Previous research determined the influence of only single anodizing parameter on the electrochemical and adsorption properties of TNT without proving the viability of determined dependences.

Despite numerous papers published over past years regarding materials with novel microstructure for applications in biosensing, there has been little research done on TNT – based electrochemical biosensors [12-16]. The most frequently reported measurement based on TNT functionalized other nanomaterials allow to achieve very low limit of detection but there has been no attempt to determine how the formation process of TNT influence onto the biosensor response.

The most sensitive electrochemical biosensor for detection of H_2O_2 was developed recently by Kafi et al. [15]. Its platform consists of TiO_2 nanotubes and methylene blue onto a glassy carbon electrode. The limit detection of this biosensor was 5 nM. Another elaborated sensor, constructed by Gao et al. [17] exhibits the lowest limit detection (37.5 nM) among the sensor using Th as a mediator. Their H_2O_2 biosensor is based on gold nanoparticles (GNPs)/thionine/GNPs/multi-walled carbon nanotubes (MWCNTs)-chitosans composite. The record sensitivity in H_2O_2 detection was achieved by A.V. Mokrushina et al. using macroporous microelectrode modified by Prussian Blue [18].

Horseradish peroxidase, enzyme commonly used for H_2O_2 detection is an electron acceptor and catalyst in many oxyda-

* UNIVERSITY OF ZIELONA GORA, DEPARTMENT OF MECHANICAL ENGINEERING, BIOMEDICAL ENGINEERING DIVISION, 9 LICEALNA STR., 65-417 ZIELONA GORA, POLAND

Corresponding author: k.arkusz@ibem.uz.zgora.pl

tion reactions [19]. Its activity is based on the high-yielding biocatalytic reduction of hydrogen peroxide. Chemically, HRP is a metalloprotein containing a heme prosthetic groups and a central iron atom. Due to the small size of HRP, which allows it to easily penetrate into the cells the enzyme is useful in qualitative assays. High purity and low cost of HRP make its use very popular. Due to that, biosensors based on HRP are widely used in medical diagnostics, biological science, analytical chemistry and environmental science [20-23]. For analytical purposes a variety of immobilization methods, such as adsorption, covalent binding, entrapment in a porous matrix have been used to improve the stability and activity of HRP on electrode surface [24].

In this work, we checked the influence of two different electrolytes: phosphoric acid and ethylene glycol on direct immobilization of enzymes on Ti/TiO_2 used as a platform for hydrogen oxide biosensors. The influence of chemical composition of the surface layer containing phosphates and fluorides was considered. The presence of fluorides in surface layer of TiO_2 nanotubes influences on the physisorption process of HRP on TNT and also on the semiconductive properties of TNT improved by thermal modification.

2. Experimental

2.1. Reagents

Titanium foil (0.25 mm thick), all chemicals and solvents were purchased from Sigma-Aldrich (UK). Horseradish peroxidase, potassium ferricyanide $K_3[Fe(CN)_6]$), acetate thionine and hydrogen dioxide (H_2O_2) were stored at 4°C and used as received. All electrochemical experiments were performed in phosphate buffered saline (PBS, 0.01 M, pH 7.4).

2.2. Preparation of titanium dioxide nanotubes

To prepare the biosensor Ti/TNT platform the titanium foils were anodized in organic (85% ethylene glycol + 0.6 % wt. NH_4F) or inorganic solution (1 M H_3PO_4 + 0.3 % wt. HF). At the beginning the foil was potentiodynamically polarized with scan rate of 0.5 V/s up to the selected potential and then it was kept at that potential for further time in the same electrolyte. Formation parameters are shown in Table 1.

Prepared electrodes were thermally modified by annealing in argon at 550°C for 2 h. Field emission scanning electron microscopy (FESEM, JEOL JSM-7600F) and energy-dispersive X-ray spectroscopy (EDS, Oxford INCA) were used to investigate surface morphology and chemical composition.

The prepared TNT arrays are hereinafter designated as: TNT/GLY for formed in ethylene glycol electrolyte, TNT/GLY/Ar for formed in ethylene glycol electrolyte and annealed in argon, TNT/H_3PO_4 for formed in H_3PO_4 electrolyte and TNT/H_3PO_4/Ar for formed in H_3PO_4 electrolyte and annealed in argon.

TABLE 1

Parameters of formation TNT in organic or inorganic electrolyte measuring around 50 nm of diameters and about 1000 nm of thickness

Voltage [V]	Time [s]	Electrolyte composition
12	7200	1 M H_3PO_4 + 0.3% wt. HF
17	3750	85% ethylene glycol + 0.6% wt. NH_4F

2.3. Immobilization of horseradish peroxidase onto TNT surface

HRP alone or with Th were immobilized on the surface of prepared electrodes using dip coating methods for 48h. Accordingly, the electrodes were immersed into the phosphate buffered saline (PBS, 0.01 M, pH 7.4) with 0.1 M HRP or with 0.1 M HRP and 0.01 M Th. The efficiency of the HRP immobilization (% of the enzyme attached to the TNT layer) were evaluated basing on the spectrophotometric analysis (Hitachi UV-Vis UV2310II) of the slops on every stage of the immobilization process at 403 nm.

2.4. Apparatus and measurements

Scanning electron microscopy (SEM) and EDS analysis were performed using JEOL 7600F with EDS analyzer (Oxford INCA). Electrochemical impedance spectroscopy and cyclic voltammetry measurements were carried out with AUTOLAB PGSTAT 302N EcoChemie, Netherlands. Cyclic voltammetry and amperometric experiments were performed in a three-electrode electrochemical cell. The Ti/TNT electrodes, immobilized with HRP or both HRP and acetate thionine were used as the working electrodes (5 mm × 5 mm, with an effective reaction area of 25 mm^2), a standard $Ag/AgCl^-$ silver chloride electrode as the reference electrode ($E_{Ag/AgCl^-}$ = 0.197 V vs. SHE at 25°C), and platinum foil (10 mm × 10 mm) as the auxiliary electrode. The 0.01 mM H_2O_2 solution was added to PBS electrolyte to detect its electrochemically. All the electrochemical experiments were carried out at room temperature.

3. Results and discussion

Titania nanotubes were fabricated by anodization method which led to an aligned array with an adjustable morphology that could be optimized for its various application among the other fabrication methods. To create different engineered architectures, the effects of electrolyte solution on the anodization of titanium foil were studied. A titanium foil was anodized in two different electrolyte solution: aqueous (H_3PO_4) and nonaqueous (ethylene glycol), both containing fluorides due to two competitive reactions [25], according to:

$$Ti + 2H_2O \rightarrow TiO_2 + 4H^+ + 4e \quad (1)$$

$$TiO_2 + 4H^+ + 6F^- \rightarrow TiF_6^{2-} + 2H_2O \quad (2)$$

The TNT anodized in nonaqueous organic electrolyte can be grown longer, while maintain smooth uniform tube architecture (ripple free) [26]. Ethylene glycol was choosen due to the low viscous and diffusion resistance, compared to other polyhydric alcohol (i.e. glycerol).

The morphology and dimensions of TiO_2 nanotubes play critical roles in determining their performance, therefore the diameter and length of TNT analyzed in this work was identical. The diameter 50 nm is regarded to be the most favorable to direct immobilization [27-28], and the length 1000 nm is the maximum length of the nanotubes limited by the high rate of titanium dioxide dissolution of HF based electrolyte [29].

3.1. Microscopy analysis of Ti/TNT platform

Fig. 1 shows SEM pictures of the TiO_2 nanotubes formed by anodizing according to applied parameters (Table 1) in two solutions: organic and inorganic. Obtained nanotubes of diameter about 50±5 nm were uniform and thickness of their layer was about 1000±50 nm. From the SEM images, it is seen that arrays of opened from the top, closed at the bottom and vertically oriented, regular nanotubes cover completely the titanium foil surface. Both, the TNT/GLY/Ar and the TNT/H_3PO_4/Ar samples show undamaged layer of nanotubes after annealing, at least within the resolution of the SEM technique.

In Table 2 the results of EDS microanalysis for samples formed in both electrolytes and thermally modified in argon are presented. The results show different concentrations of elements in surface layer of nanotubes according to formation conditions.

TABLE 2

Results of EDS analysis of nanotube layers formed in organic or inorganic electrolyte and annealed in argon

	TNT/H_3PO_4	TNT/H_3PO_4/Ar	TNT/GLY	TNT/GLY/Ar
Ti [%]	66.23	63.18	60.48	63.01
O [%]	28.55	30.09	29.27	36.99
F [%]	6.47	3.81	10.25	—

It can be seen that annealing in argon caused an increase of oxygen content by about 7% for TNT formed in ethylene glycol solution and about 2% for H_3PO_4 solution. The possible explanation is the reduction of tetravalent titanium Ti^{4+} to Ti^{3+} cations [25,29] and the formation of oxygen vacancies. Due to the ability to migrate and intercalate into the oxide films during the anodizing, the presence of fluoride, as a residue from the electrolyte is observed. TNT/GLY contains much more fluoride in nanotubular oxide layer than the other samples, most likely due to the higher pH, concentrated fluoride electrolyte and smoother surface of nanotubes [30]. Interesting is that annealing in argon results in the disappearance of fluorides from samples formed in ethylene glycol, what is desired in biosensing because it is known that F^- anions are inhibitors of native HRP [31].

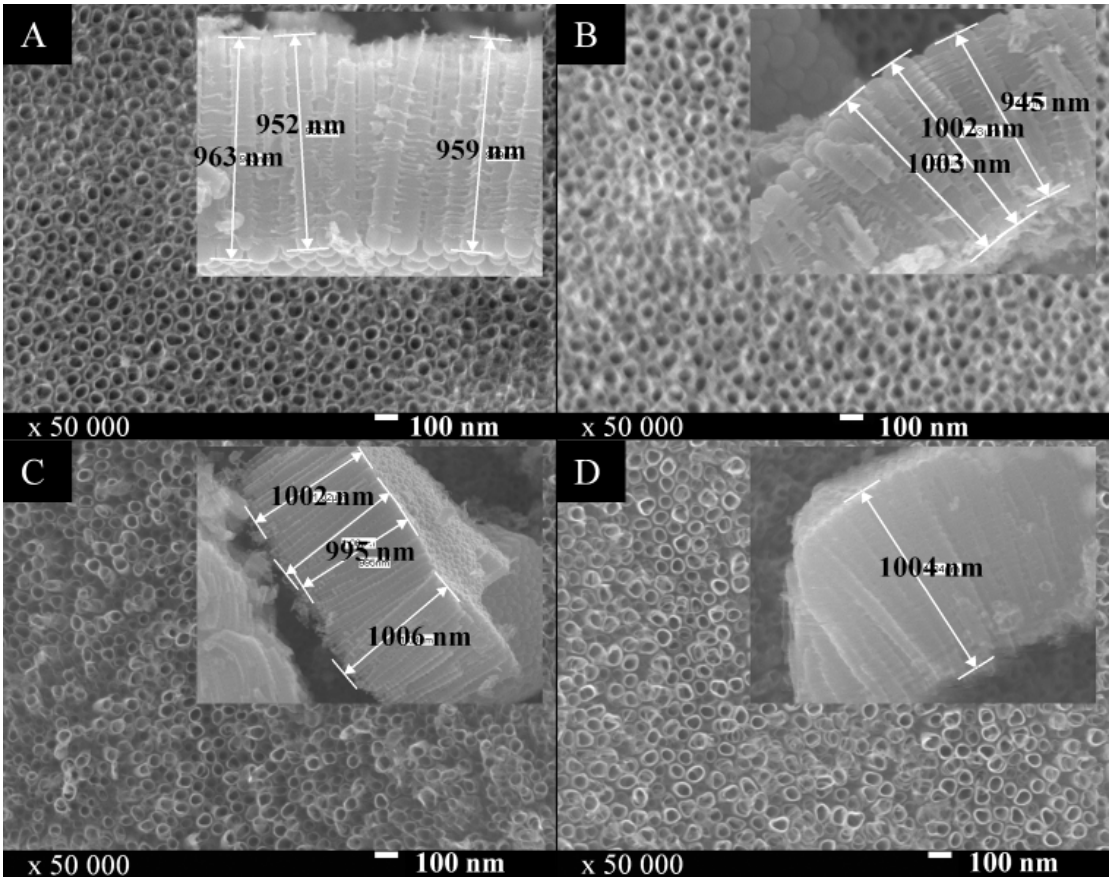

Fig. 1. SEM top-view and cross-sectional images of TNT/H_3PO_4 (a), TNT/H_3PO_4/Ar (b), TNT/GLY (c), TNT/GLY/Ar (d)

3.2. Open Circuit Potential (OCP) of Ti/TNT

The electrochemical characteristics of annealed and non-annealed titanium nanotubes were examined by open circuit potential measurements. Samples were immersed in PBS (0.01 M, pH 7.4) for 30 min. The OCP curves shown in Fig. 2 are stable.

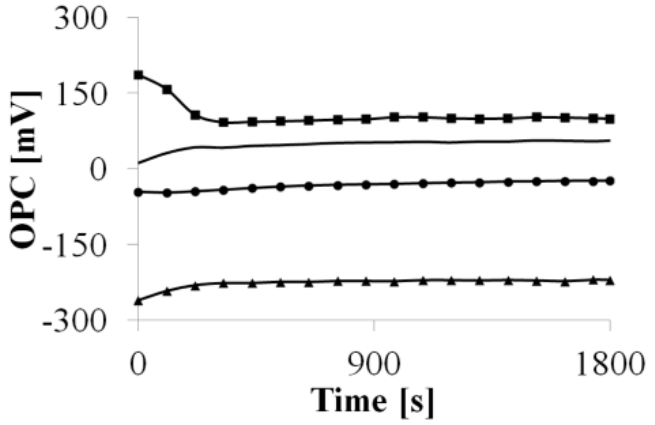

Fig. 2. Open circuit potential (E_{OPC}) of TNT/H_3PO_4 (circle), TNT/H_3PO_4/Ar (square), TNT/GLY (up triangle) and TNT/GLY/Ar (solid line) measured in 0.01 M PBS for 30 min

TNT formed in organic solution immersed in PBS exhibit a constant OCP during the stabilisation stage, showing a thermodynamic trend similar to oxidise. Small current oscillations seen on OCP curves for TNT formed in ethylene glycol electrolyte may suggest ongoing oxidation and metastable nature of nanotubular oxide layers.

In contrast, a cathodic shift was observed on TNT formed in inorganic solution after its immersing in PBS solution. Adsorption of alkaline metal cations of salts (Na^+, K^+) on TNT surface blocks its free site and decreases the overall corrosion rate, due to the growth of a less stable oxide with lower protective properties.

Before the annealing, higher OCP value was observed for TNT/H_3PO_4 (-0.024 V vs. Ag/AgCl), than for TNT/GLY (-0.22 V vs. Ag/AgCl). Organic electrolytes with F^- ion additions make chemical dissolution of nanotubes layer and mobility of F^- ions lower. The current efficiency for TNT formation is significantly higher than compared to inorganic electrolytes, due especially to the change of viscosity [32].

Annealing in argon causes the increase of the OCP value (E_{OPC}) for Ti/TNT layers formed in organic and inorganic electrolyte comparing to the stationary potential of non-annealed samples. It is related to the higher fluoride concentrations, shifting OCP towards more cathodic values in both materials. Annealing in argon causes decrease/reduction of fluoride resulting in more positive OCP values of thermally modified TNT, according to fluorides concentration (Table 2). Shift of the OCP potentials to more positive values is favorable for the immobilization of enzyme on the electrode surface. The basic amino acid residues (e.g. HRP) exhibit negative charges in PBS (0.01 M, pH 7.4). The negatively charged protein molecules are easily pulled to the positive matrix of biosensor [33].

3.3. EIS measurements of Ti/TNT

The electrochemical impedance spectroscopy tests of the prepared samples were recorded in PBS solution (0.01 M, pH 7.4) in the frequency range 0.1-10.000 Hz and the amplitude 0.01 V. The impedance spectra for samples formed in different electrolytes and thermally modified are shown in Fig. 3.

Nyquist diagram (Fig. 3a), illustrating the impedance of surface layer for samples formed in 85% ethylene glycol + 0.6% wt. NH_4F and 1 M H_3PO_4 + 0.3% wt. HF, respectively both annealed in argon, presents large circle-shaped curves, which are characteristic for thin oxide layers. The decrease of the radius of semi-circle recorded for thermally modified TNT (Fig. 3a) confirm increased electrolytic resistance of the electrolyte, what is associated with the presence of fluoride (Table 2.) and interaction between the electrolyte and TNT layers. The highest electric resistance was recorded for TNT/H_3PO_4, whereas the lowest electric resistance for TNT/GLY/Ar samples.

These tendencies of impedance changes are clearly shown in Bode charts (Figs. 3b and 3c). One time constant in impedance spectra seen in Fig. 3c indicates that the surface film is built of one nanotubular layer of titanium dioxide formed by anodizing. It can be seen that annealing in argon in temperature 550^{o}C during 2h causes TNT layer homogenerity increase by decreasing the -Zphase values (Fig. 3c) for TNT formed both in organic and inorganic solutions. TNT/GLY/Ar is the layer characterized by the lowest resistance (Fig. 3a) and the highest impedance (Fig. 3b) and also the highly uniform surface layer (Fig. 3c). Thermal modification of TNT under argon shows lack of oxygen in the surface, which proves its deficiency and the presence of oxygen vacancies [34]. The highest intensity of signals confirming the presence of TiO_2 titanium, Ti_2O_3, Ti^{3+} were also recorded for those samples, which is preferable for electric conductivity.

The results of impedance investigations were fitted to the equivalent circuit (Fig. 3d), which represents bi-layer model – titania nanotubes and interior of the TNT. The Rs element represents the uncompensated solution resistance. Parallel combination R1C1 represents the resistance and capacitance of the porous TiO_2. The next parallel combination R2 and the constant phase element (CPE-Y,N) determining TiO_2 nanotubes layer leads to a depressed semicircle in the corresponding Nyquist impedance plot (Fig. 3a) [31]. The residual component of this circuit – parallel connection R3 and CPE1 represents the resistance and capacitance of the biological layer immobilized on the TNT.

The parameters determined by fitting of the experimental EIS data are summarized in Table 3. The resistance, R_s,of the TNT electrodes changed in the following order: 55 Ω (TNT/GLY) > 34 Ω (TNT/H_3PO_4) > 31 Ω (TNT/H_3PO_4/Ar) > 10.7 Ω (TNT/GLY/Ar), while the electrical capacity (C1) in order: 11.6 μF (TNT/GLY/Ar) > 6.34 μF (TNT/H_3PO_4/Ar) > 2.16 μF (TNT/GLY) > 1.67 μF (TNT/H_3PO_4). These results also confirm that the TNT formed in 85% ethylene glycol + 0.6% wt. NH_4F and annealed in argon possesses the lowest electrolyte resistance and the higher electrical conductivity.

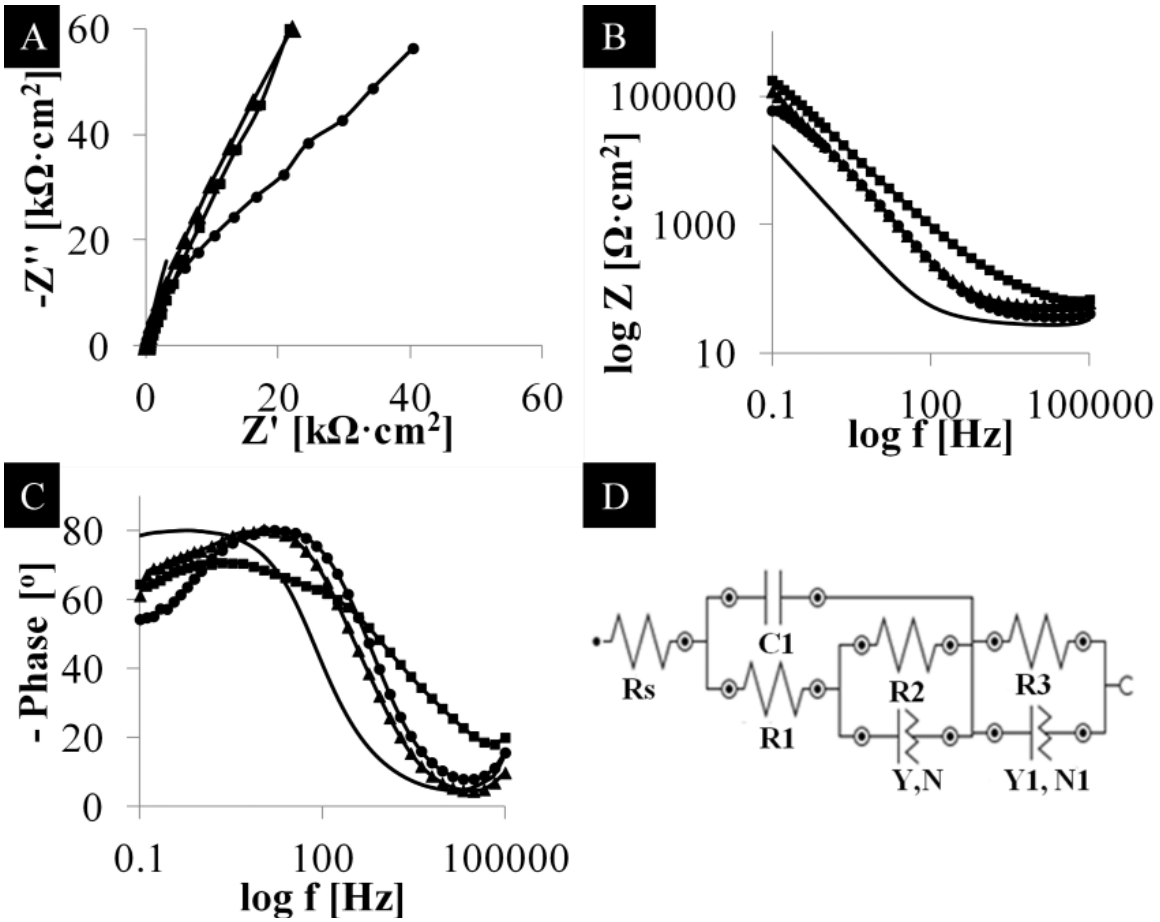

Fig. 3. EIS spectras of TNT/H_3PO_4 (circle), TNT/H_3PO_4/Ar (square), TNT/GLY (up triangle) and TNT/GLY/Ar (solid line) electrodes recorded at the potential of 0.01 V in 0.01 M PBS; a) Nyquist plot, b) and c) Bode plots, d) the equivalent circuit used in the simulation, where Rs – the ohmic resistance of the electrolyte; C1, R1 – capacitance and resistance for porous layer; CPE1, R2 – constant phase element and resistance of double layer; CPE2, R3 – constant phase element and polarization resistance of immobilized enzyme

TABLE 3

Selected impedance components for TiO_2 nanotubes electrodes determined by fitting EIS experimental data using the equivalent circuit shown in Fig. 3d

Electrodes	x^2	Rs [Ω]	C1 [μF]	R1 [Ω]
TNT/GLY	0.15	55	2.16	648
TNT/GLY/Ar	0.02	10.7	11.6	18
TNT/H_3PO_4	0.06	34	1.67	862
TNT/H_3PO_4/Ar	0.11	31	6.34	1910

3.4. Cyclic voltammetry of Ti/TNT

Cyclic voltammetry tests (CV) for Ti/TNT, formed in different electrolytes and thermally modified (Fig. 4a), were carried out in PBS (0.01 M, pH 7.4) for potential ranging from –1 V÷1 V vs. Ag/AgCl with scan rate 0.05 V/s. No oxidation or reduction peaks are seen on the voltammograms. Higher anodic and cathodic current values were measured for samples modified in argon formed in two types of electrolyte. It may be a result of ionic affinity of TiO_2 towards electrolyte components.

The phenomena occurring at the metal-semiconductor boundary depend on the potential and space-charge layers near the semiconductor surface. Increased current values at approx. -0.8 V refer to the redox reaction: $Ti^{4+} + e \rightleftharpoons Ti^{3+}$. Kavan [35] suggests that it corresponds to the reduction of impurities, such as H_2O or O_2. It may also be caused by the accumulation layer on n-type semiconductor, which is characterized by an abundant number of charges (electrons) in the near-surface layer of TiO_2. Electrons moving up to the surface have higher energy and the TNT layer exhibits capacitive effect. Formation of the surface space charge region depleted by mobile charge carriers is related to rectangular potential barrier and bending of energy bands. The presence of an electron-rich layer at the surface of TNT confirms the electrical conductivity of formed layer [10]. Increasing values of current in the range –1÷–0.75 V may also be caused by diffusion of ions in porous materials as confirmed by the difference between the cathodic and anodic current.

The electrochemical properties of TNT electrodes were also investigated by cyclic voltammetry in 10 mM $K_3[Fe(CN)_6]$ with PBS (Fig. 4b). The measurements were carried out in the potential range of –1÷1 V vs. $Ag/AgCl^-$ at the same sweep rate of 0.05 V/s. The redox couple of $Fe(CN)_6^{3-}/Fe(CN)_6^{4-}$ appears reversibly on voltammograms for TNT/GLY/Ar samples. Obtained current peaks are then well-defined with Ipa/Ipc = 0.82, and a peak separation of 0.45 V is observed. The formal potential

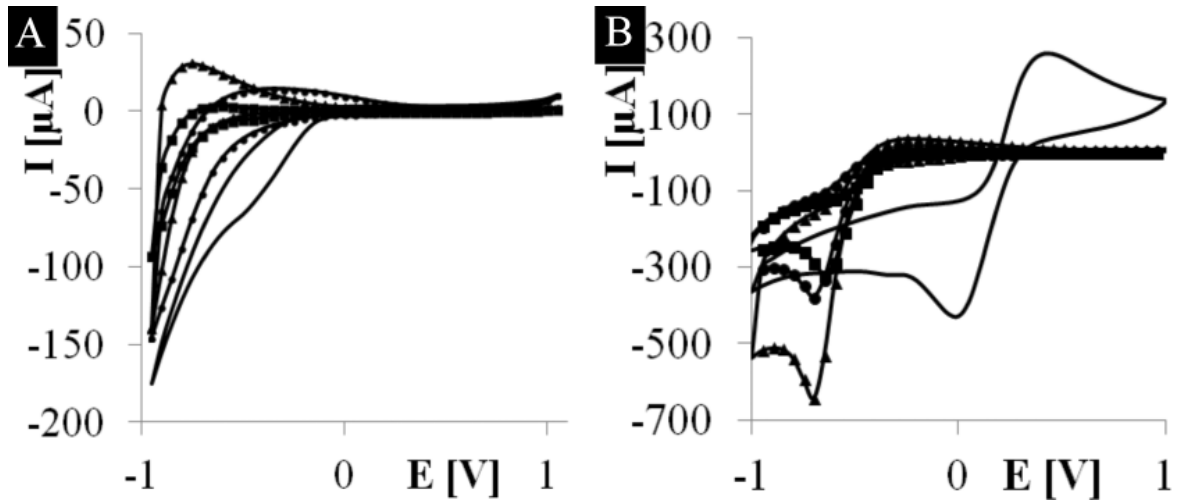

Fig. 4. Cyclic voltammograms of TNT/H_3PO_4(circle), TNT/H_3PO_4/Ar (square), TNT/GLY (up triangle) and TNT/GLY/Ar (solid line) electrodes measured in 0.01 M PBS (a) containing 10 mM $K_3[Fe(CN)_6]$ (b). Scan rate: 0.05 V/s

values of the observed peaks are shifted towards the cathodic direction corresponding to the open circuit potential of samples (~50 mV vs. Ag/AgCl). They are well correlated with redox potential of $K_3[Fe(CN)_6]$ (E_0 = 0.436 V at pH 7.0) [36]. The cyclic voltammograms of $K_3[Fe(CN)_6]$ at TNT/GLY, TNT/H_3PO_4, TNT/H_3PO_4/Ar show much lower signals.

3.5. Electrochemical characteristics of H_2O_2 biosensor

Electrochemical detection of H_2O_2 based on Ti/TNT were carried out using HRP alone and HRP with thionine acetate. Both reagents were immobilized on the Ti/TNT by drop coating for 48h. The efficiency of the immobilization (% of the enzyme

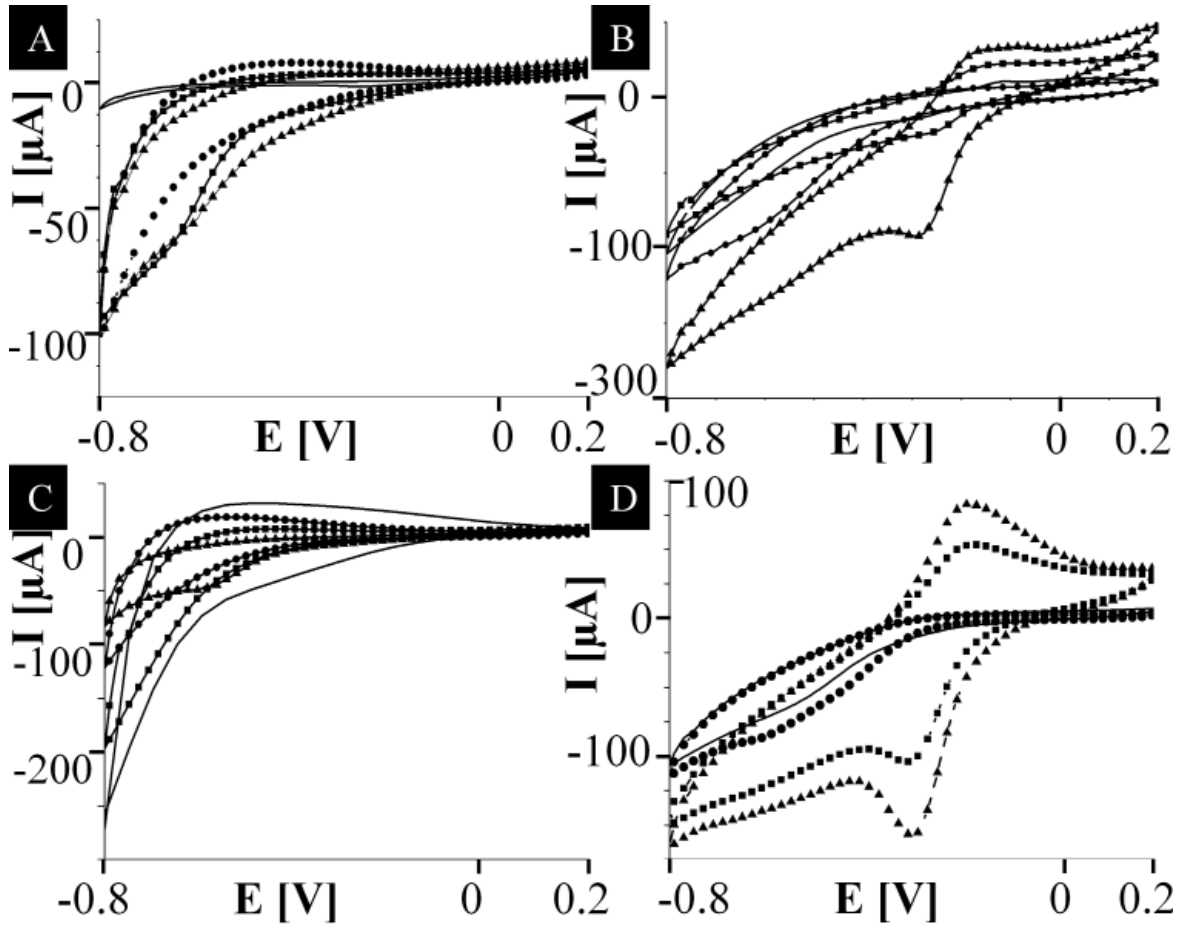

Fig. 5. Cyclic voltammograms of TNT/H_3PO_4(a), TNT/H_3PO_4/Ar (b), TNT/GLY (c) and TNT/GLY/Ar (d) electrodes measured in 0.01 M PBS (solid line) containing: 0.1 M HRP, 0.01 mM H_2O_2 (circle); 0.1 HRP, 0.01 M acetate thionine, 0.01 mM H_2O_2 (up triangle) with scan rate 0.05 V/s

attached to the platform surface) were evaluated basing on the spectrophotometric analysis of the slops on every stage of the immobilization process. The voltammograms for the prepared TNT electrodes (Fig. 5), recorded in PBS solution, show a flat wave which typically illustrates behavior of nanotubular titanium dioxide surface in the absence of the redox couple [29]. No cathodic or anodic peaks were observed in voltammograms for HRP immobilized on TNT. To improve the biosensing ability the mediators – acetate thionine and HRP were applied in further studies.

As it can be seen in Fig. 5b, 5d, current observed in voltammograms for TNT/GLY/Ar and TNT/H_3PO_4/Ar increases due to advantageous changes in conductivity of semiconductive material caused by thermal modification in argon. The immobilization of HRP and acetate thionine resulted in the appearance of peaks and the increase of the current.

Upon the addition of the hydrogen peroxide to the electrochemical cell (Fig. 6), only TNT/H_3PO_4/Ar and TNT/GLY/Ar displays a pair of redox and oxidation peaks. The reduction peaks appear at –0.15 V (vs. Ag/AgCl) and at –0.2 V (vs. Ag/AgCl) and the oxidation peaks at –0.28 V (vs. Ag/AgCl) and at –0.3V (vs. Ag/AgCl) for TNT/H_3PO_4/Ar and TNT/GLY/Ar, respectively. For TNT/GLY/Ar the peaks separation amounts to 0.1 V and for TNT/H_3PO_4/Ar amounts to 0.13 V.

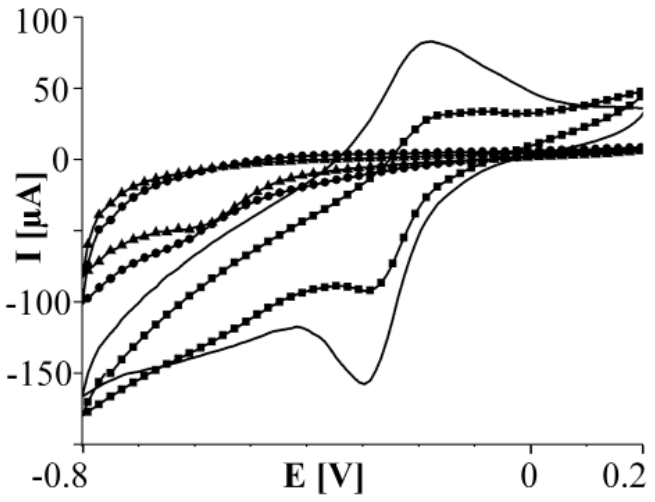

Fig. 6. Cyclic voltammograms of TNT/H_3PO_4(circle), TNT/H_3PO_4/Ar (square), TNT/GLY (up triangle) and TNT/GLY/Ar (solid line) electrodes measured in 0.01 M PBS (solid line) containing 0.1 M HRP, 0.01 M acetate thionine and 0.01 mM H_2O_2 with scan rate 0.05 V/s

The above peaks correspond to a typical electron transfer between the H_2O_2 and the HRP molecule [37]:

$$HRP_{red} + H_2O_2 + 2H^+ \rightarrow HRP_{ox} + 2H_2O \quad (3)$$

$$HRP_{ox} + Th \rightarrow HRP_{red} + Th^+ \quad (4)$$

$$Th^+ + 2e^- + H^+ \rightarrow Th \quad (5)$$

Net reaction: $$H_2O_2 + 2e + 2H^+ \rightarrow 2H_2O \quad (6)$$

Very often the metal redox center, i.e. the iron heme group in HRP enzyme in which the electron transfer can be achieved through the Fe(III) to Fe(II) redox reaction, is hidden inside large molecules of protein and located far away from the electrode surface. Considering the low values of diffusion coefficient and possible denaturation of enzyme/protein complex adsorbed on the electrode surface, the electrical communication of the metal redox centers with electrode surface is a key factor in the elaboration of enzymatic biosensors. The Ti/TNT metal/semiconductor nanotubes system, owns this special feature of the effective electrical contact and electron-transfer reaction with electrodes, as has been proved in our investigation.

3.6. Electrochemical response to hydrogen peroxide

The calibration curves for biosensor based on TNT/GLY/Ar as a platform in Fig. 7 represented by a linear regression show that the prepared platform was sensitive to H_2O_2 in PBS solution. A limit detection of 3 μM of H_2O_2 was obtained with a good reproducibility for the developed biosensor. The obtained limit detection was higher than the obtained by other methods [20-23, 38-39]. The biosensor response depended on the conductivity and the large surface-to-volume ratio attained with titania nanotubes.

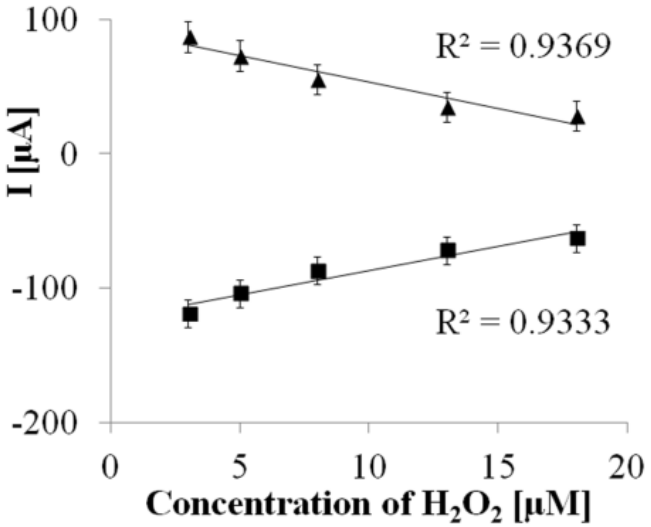

Fig. 7. Cathodic (up triangle) and anodic (square) peaks for cyclic voltammetry of TNT/GLY/Ar electrode measured in 0.01 M PBS (solid line) containing 0.1 M HRP, 0.01 M acetate thionine and varying concentration of H_2O_2 with scan rate 0.05 V/s

4. Conclusion

Titania nanotubes formed in ethylene glycol solution (85% ethylene glycol + 0.6% wt. NH_4F) and annealed in argon showed that the prepared porous structure considerably stimulated the hydrogen peroxide biosensor response.

The thermal treatment in argon of TNT formed in organic and inorganic did not influence nanotubes morphology and their tubular shape, but caused different amperometric and impedance characteristics. A limit detection of 3 μM of H_2O_2 was obtained with a good reproducibility of the developed biosensor

based on TNT/GLY/Ar as a platform. Obtained results may be promising to use this electrode as a platform for other highly sensitive sensors.

Acknowledgement

The authors gratefully thank for the financial support received by the Ministry of Science and Higher Education in the Diamond Grant (no DI2011 004941).

REFERENCES

[1] C. Yua, L. Wanga, W. Li, C. Zhub, N. Baoa, H. Gua, Sens. Actuators B Chem. **211**, 17-24 (2015).
[2] Y. Wang, H. Xu, J. Zhang, G. Li, Sensors **8**, 2043-2081 (2008).
[3] H. Liu, V. Gu, D. Li, M. Zhang, Mater. Res. Bull. **64**, 375-379 (2015).
[4] R. Major, M. Sanak, P. Wilczek, J.M. Lackner, M. Kot, B. Major, Nanostructural materials for implants and cardiovascular biomedical devices, in: Z. Nawrat (Ed.), 2011 ImplantExpert.
[5] P. Handzlik, K. Fitzner, Arch. Metall. Mater. **55** (2), 521-532 (2010).
[6] P. Xiao, B.B. Garcia, Q. Guo, D. Liu, G. Cao, Electrochem. Commun. **9**, 2441-2447 (2007).
[7] S. Bauer, S. Kleber, P. Schmuki, Electrochem. Commun. **8**, 1321-1325 (2006).
[8] P. Hoyer, Langmuir **12**, 6, 1411-1413 (2006).
[9] H. Ou, S.L. Lo, Sep. Purif. Technol. **58**, 1, 179-191 (2007).
[10] A. Kaczmarek, T. Klekiel, E. Krasicka-Cydzik, Surf. Interface Anal. **42**, 510-514 (2003).
[11] E. Krasicka-Cydzik, K. Arkusz, A. Kaczmarek, Eng. Biomat. **15**, 114, 34-40 (2012).
[12] E. Krasicka-Cydzik, A. Kaczmarek, K. Arkusz, Mater. Eng. **4**, 485-489 (2011).
[13] Y. Xie, L. Zhoua, H. Huang, Biosens. Bioelectron. **22**, 2812-2818 (2007).
[14] S. Liu, A. Chen, Langmuir **21**, 8409-8413 (2005).
[15] A.K.M. Kafi, G. Wu, A. Chen, Biosens. Bioelectron. **24**, 566-571 (2008).
[16] I. Roman, M.L. Soare, R.D. Trusca, C. Fratila, E. Krasicka-Cydzik, M.S. Stan, A. Dinischiotu, J. Electrochem. Soc. **161** (14) 275-282 (2014).
[17] C. Gao, F. Hua, C.M. Li, P.K. Shenc, Biosens. Bioelectron. **24**, 819-824 (2008).
[18] A.V. Mokrushina, M. Heim, E.E. Karyakina, A. Kuhn, A.A. Karyakin, Electrochem. Commun. **29**, 78-80 (2013).
[19] A. Cordoba, N. Alasino, M. Asteasuain, I. Magario, M.L. Ferreira, Chem. Eng. Sci. **129**, 249-259 (2015).
[20] X. Yin, M. Guo, Y. Xia, W. Huang, Z. Li, J. Electroanal. Chem. **720**, 19-23 (2014).
[21] B. Lyson-Sypien, K. Zakrzewska, M. Gajewska, Arch. Metall. Mater. **60** (2) 935-940 (2015).
[22] H. Tavakoli, A.A. Baghbanan, Bioelectrochem. **104**, 79-84 (2015).
[23] S. Li, X. Zhu, W. Zhang, G. Xie, W. Feng, Appl. Surf. Sci. **258**, 2802-2807 (2012).
[24] E.E. Ferapontova, Electroanalysis **16** (13), 1101-1112 (2004).
[25] P. Roy, S. Berger, P. Schmuki, Angew. Chem. Int. Ed. **50**, 2904-2939 (2011).
[26] M.R. Sturgeon, P. Lai, M.Z. Hu, J. Material. Res. **26** (20), 2612-2623 (2011).
[27] S. Oh, K.S. Brammer, Y.S. J. Li, D. Teng, A. Engler, S. Chien, A. Jin, PNAS, **106** (7), 2130-2135 (2009).
[28] E. Gongadze, D. Kabaso, S. Bauer, P. Jung, P. Schmuki, A. Iglic, Mini Rev. Med. Chem. **13** (2), 194-200 (2013).
[29] J. Kapusta-Kołodzieja, O. Tynkevych, A. Pawlika, M. Jarosz, J. Mech, G.D. Sulka, Electrochim. Acta **144**, 127-135 (2014).
[30] B. Yang, C.K. Ng, M.K. Fung, C.C. Ling, A.B. Djurisic, S. Fung, Mat. Chem. Phys. **130**, 1227–1231 (2011).
[31] P. Xiao, D. Liu, B.B. Garcia, S. Sepehri, Y. Zhang, G. Cao, Sens. Actuators B Chem. **134**, 367-372 (2008).
[32] M. Ramalingam, S. Ramakrishna, S. Best, Biomaterials and Stem Cells in Regenerative Medicine, 2012 CRC Press.
[33] E. Ferapontova, E. Dominguez, Bioelectrochem**. 55**, 127-130 (2002).
[34] M. A. Henderson, Surf. Sci. **419**, 2 (1999).
[35] L. Kavan, M. Grätzel, J. Rathouský, A. Zukal, J. Electrochem. Soc. **143**, 394 (1996).
[36] P.G. Simt, E. Whalley, J. Phys. Chem. **91**, 1877-1878 (1987).
[37] T. Ruzgas, E. Csöregi, J. Emnéus, L. Gorton, Anal. Chim. Acta. **330** (2-3), 123-138 (1996).
[38] F. Wu, J. Xu, Y. Tian, Z. Hu, L. Wang, Y. Xian, L. Jin, Biosens. Bioelectron. **24**, 198-203 (2008).
[39] A. Curulli, A. Cusma, S. Kaciulis, G. Padeletti, L. Pandolfi, F. Valentini, M. Viticoli, Surf. Interface Anal. **38**, 478-481 (2006).